BULLETIN OF THE POLISH ACADEMY OF SCIENCES
TECHNICAL SCIENCES, Vol. 74(1), 2026, Article number: e155898
DOI: 10.24425/bpasts.2025.155898

Development of low-emission photocatalytic cement composites with co-ground TiO_2-fly ash and TiO_2-calcium carbonate systems

Agnieszka ŚLOSARCZYK[1]*, Izabela KLAPISZEWSKA[1], Patryk JĘDRZEJCZAK[1], Marta THOMAS[1], and Łukasz KLAPISZEWSKI[2,3]**

[1] Institute of Building Engineering, Faculty of Civil and Transport Engineering, Poznan University of Technology, PL-60965 Poznan, Poland
[2] Institute of Chemical Technology and Engineering, Faculty of Chemical Technology, Poznan University of Technology, PL-60965 Poznan, Poland
[3] Interdisciplinary Centre for Ecotechnology, Poznan University of Technology, PL-60965 Poznan, Poland

Abstract. This study presents an innovative method for producing low-emission cement composites with photocatalytic properties by partially replacing Portland cement with fly ash, ground granulated blast furnace slag, and calcium carbonate. Novel ground systems combining fly ash-TiO_2 or calcium carbonate-TiO_2 were synthesized via high-energy ball milling to enhance dispersion and minimize TiO_2 agglomeration. The modified composites exhibited improved hydration kinetics, including reduced setting times and up to 50% lower cumulative hydration heat. Mechanical tests confirmed comparable or superior compressive and flexural strengths as compared with the reference materials. All TiO_2-containing composites showed UV-induced photocatalytic activity, with anatase-based systems yielding the best results. Carbon footprint analysis confirmed the environmental benefits, particularly in reducing CO_2 emissions. These findings support the development of multifunctional, sustainable cementitious materials for eco-efficient construction.

Keywords: low-emission composites; titanium dioxide; calcium carbonate; fly ash; photocatalytic activity.

1. INTRODUCTION

Low-emission cementitious composites, despite their significant role in reducing carbon dioxide emissions and their environmentally friendly characteristics, are associated with several challenges currently faced by researchers. Among these, relatively low early-age strength is of particular concern. Cement mortars in which Portland cement has been substantially replaced with fly ash often exhibit poor early-age strength. This phenomenon has been demonstrated in the study by Huseien *et al*. [1], who replaced 50% of the cement with fly ash. It is generally acknowledged that the most favorable strength parameters are achieved in composites where the fly ash content does not exceed 20–30%. Increasing the proportion of fly ash leads to a reduction in both density and thermal conductivity [2]. For mortars containing 20% fly ash, an increase in compressive strength after 28 days of curing has been demonstrated, along with a reduction in CO_2 emissions [3]. In terms of flexural strength, a 10% fly ash content yields the most advantageous results, while further increases result in a decline in performance [4]. However, considering both the preservation of relatively high mechanical strength and the maximization of CO_2 emission reduction, the optimal fly ash replacement level is in the range of 20–30% [3, 5].

One of the methods for enhancing the reactivity of fly ash – and consequently the final mechanical properties of cementitious composites – is the grinding of fly ash to reduce its particle size. The authors of study [6] demonstrated that mortars containing 20%, 40% and 60% ball-milled fly ash exhibited a significant improvement in mechanical properties. Similar observations were made by the authors of study [7], who compared composites made with unground fly ash and ultrafine fly ash, replacing up to 50% of the cement. The results obtained by the researchers showed that mortars containing ultrafine fly ash exhibited significantly higher mechanical properties at both early and later stages of curing.

In the production of multicomponent cements, in addition to the already discussed fly ash, ground granulated blast furnace slag (GGBFS) [8, 9] and limestone (calcium carbonate) are also commonly used, with the latter contributing to CO_2 emission reduction by lowering the clinker content in the final cement product [10]. The use of calcium carbonate nanoparticles may contribute to the improvement of compressive strength in cement mortars. In study [11], it was demonstrated that a 1 wt.% addition of $CaCO_3$ nanoparticles led to a 22% increase in compressive strength as compared to the composite without the addition. Additionally, the porosity and microstructure analysis of the resulting mortars showed a reduction in pore volume and a more compact microstructure. The presence of $CaCO_3$ also positively influences workability of the mortar and promotes early hydration and strength development [12, 13].

In response to the urgent need to intensify research on functional cement composites with significantly reduced CO_2 emis-

*e-mail: agnieszka.slosarczyk@put.poznan.pl
**lukasz.klapiszewski@put.poznan.pl

Manuscript submitted 2025-07-20, revised 2025-09-24, initially accepted for publication 2025-09-25, published in January 2026.

© 2026 The Author(s). This is an open access article under the CC BY license (http://creativecommons.org/licenses/by/4.0/)

sions, which leverage the synergistic benefits of partially replacing Portland cement clinker with fly ash, ground granulated blast furnace slag, and calcium carbonate, innovative ternary and quaternary low-emission cement composites have been developed. This study proposes the advancement of low-emission cement composites with photocatalytic properties, in which a portion of Portland cement is substituted with co-ground fly ash-TiO_2 and calcium carbonate-TiO_2 systems. These systems were produced using a high-energy ball mill and subsequently subjected to comprehensive characterization, alongside the pristine powder materials. The analyses included particle size distribution, oxide composition determined by X-ray fluorescence (XRF), and Fourier-transform infrared (FTIR) spectra, which provided insights into the chemical bonding present in the materials. In the next stage, the systems developed and raw powders were incorporated as additives in cement mortars. For the resulting composites, hydration heat, mechanical performance and microstructural characteristics of the mortars were determined. Furthermore, photocatalytic activity was evaluated, and a carbon footprint assessment of the proposed material solutions was conducted, highlighting their potential in the context of sustainable development and greenhouse gas mitigation.

2. MATERIALS AND METHODS

2.1. Materials

Low-emission cement composites were produced using Portland cement CEM I 42.5 R /CEM/ (Górażdże Cement S.A., Górażdże, Poland), quartz sand (Kwarcmix, Tomaszów Mazowiecki, Poland), fly ash /FA/ (Opole Plant, Opole, Poland), titanium dioxide (TiO_2) in anatase form /AN/ (Sigma-Aldrich, Merck, Darmstadt, Germany), titanium dioxide (TiO_2) Aeroxide® P25 (CAS number: 13463-67-7) /P25/ (Sigma-Aldrich, Steinheim am Albuch, Germany), calcium carbonate /CC/ (CHEMPUR, Piekary Śląskie, Poland), slag /SL/ and water.

Both titanium dioxides AN and P25 were first milled with calcium carbonate or fly ash using planetary ball mill PM 400 (Retsch GmbH, Haan, Germany). The detailed oxide composition, based on XRF analysis, of all of the powder materials used in the tests is summarized in Table 1.

Table 1
Oxide composition of the powders used in this study

	Powder material (%)									
	P25	AN	SL	CEM	FA	CC	FA + P25	FA + AN	CC + P25	CC + AN
MgO	–	–	6.82	1.40	1.62	0.09	1.70	1.74	0.06	0.07
Al_2O_3	–	–	9.45	3.99	29.03	–	26.23	26.26	–	–
SiO_2	–	–	34.63	16.11	50.39	–	50.78	50.62	–	–
P_2O_5	0.18	0.24	–	–	0.99	–	0.80	0.79	–	–
SO_3	–	1.26	2.14	3.90	0.89	–	0.55	0.59	–	0.09
K_2O	–	–	0.90	0.87	2.36	–	2.14	2.12	–	–
CaO	0.06	0.07	44.12	67.34	5.36	99.71	5.18	5.27	83.74	83.93
TiO_2	99.71	98.34	0.72	0.26	1.51	–	4.66	4.59	15.81	15.59
V_2O_5	–	–	0.02	0.02	0.05	–	0.05	0.05	0.07	0.07
Cr_2O_3	–	–	–	0.03	0.04	–	0.02	0.03	–	–
MnO	–	–	0.24	0.26	0.07	–	0.07	0.07	–	–
Fe_2O_3	–	–	0.63	5.46	7.18	0.02	7.36	7.40	0.02	0.02
NiO	–	–	–	–	0.01	–	0.01	0.01	–	–
CuO	–	–	–	0.02	0.02	–	0.02	0.02	–	–
ZnO	–	–	–	0.05	0.02	–	0.02	0.02	–	–
Rb_2O	–	–	–	–	0.02	–	0.01	0.01	–	–
SrO	–	–	0.08	0.12	0.14	0.01	0.13	0.13	0.01	0.01
Y_2O_3	–	–	–	–	–	–	0.01	0.01	–	–
ZrO_2	–	0.01	0.03	0.01	0.05	–	0.07	0.08	0.09	0.03
Nb_2O_5	–	0.01	–	–	–	–	–	–	–	–
Ag_2O	0.05	0.08	0.11	0.117	0.10	0.15	0.08	0.08	0.17	0.17
SnO_2	–	–	–	0.01	–	0.01	–	–	0.01	0.01
TeO_2	–	–	0.01	0.01	0.01	0.01	–	–	0.02	0.02
BaO	–	–	0.09	0.02	0.12	–	0.08	0.08	–	–
Eu_2O_3	–	–	–	–	0.04	–	0.04	0.04	–	–
PbO	–	–	–	–	0.01	–	0.01	0.01	–	–

2.2. Characterization of raw powder materials

2.2.1. Particle size distribution

The dispersive properties of all raw materials were characterized using a Zetasizer Nano ZS (Malvern Instruments Ltd., UK). Precise measurement of particles within the size range of 0.6 to 6000 nm is enabled by the non-invasive backscattering (NIBS) method that is used in this device.

2.2.2. Fourier transform infrared spectroscopy

To investigate the functional groups present in the structure of the raw powder materials, Fourier transform infrared spectroscopy was employed. Spectral data were collected using a Vertex 70 spectrometer (Bruker, Germany). The samples were prepared as potassium bromide (KBr) tablets. Measurements were conducted with a spectral resolution of 0.5 cm^{-1} across the wavenumber range of 4000 to 450 cm^{-1}.

2.2.3. X-ray fluorescence

Surface composition was analyzed by energy dispersive X-ray (EDX) and X-ray fluorescence (EDXRF). Mapping was performed with a Hitachi HT7700 (STEM mode, Thermo Scientific microanalysis system), and elemental contents were measured using an Epsilon4 EDXRF spectrometer (PANalytical, Malvern, UK).

2.3. Preparation of cement composites

The fresh mortar was prepared in accordance with PN-EN 196-1 using an automatic mortar mixer. Three recipe groups (1, 2, 3) were prepared containing 36% fly ash as the main clinker substitution, 51% slag together with 10% fly ash and 51% slag with 10% calcium carbonate correspondingly. In addition, each group was modified by doping TiO_2 with fly ash in either anatase form (AN) or Aeroxide® form (P25). The selection of these two types of TiO_2 was based on a comprehensive literature review. P25 was chosen because its powdered form exhibits significantly superior photocatalytic properties as compared to other TiO_2 forms. This performance is attributed to its crystalline structure, in which rutile nanocrystallites are dispersed within the anatase phase [14]. The second material, commercial anatase, although less active – particularly in the visible-light range – contributes, when incorporated into a cementitious matrix, to the formation of a composite with enhanced compressive and flexural strength, as well as improved microbiological purity [15]. The weight of the mixture components remained constant; however, the addition of FA, SL, CC, or TiO_2 was accompanied by a proportional reduction in the cement content. The mixture consisted of water, binder and quartz sand in a 1:2:3 ratio, with detailed binder composition provided in Table 2. Prior to mixing, all powder additives were dry-blended with the cement.

2.4. Methods applied for testing cement composites

2.4.1. Heat of hydration

To assess the heat of hydration, a semi-adiabatic method was used, carried out in accordance with EN 196-9 on an apparatus from TESTING Bluhm & Feuerherdt GmbH (Berlin, Germany). It was determined by monitoring the temperature rise of the cement mortar, which directly correlates with the kinetics of the cement hydration process.

2.4.2. Mechanical strength

Tests of flexural and compressive strength were carried out with a Servo-Plus Evolution testing machine (Matest S.p.A., Treviolo BG, Italy) in compliance with PN-EN 196-1. Flexural

Table 2
Material composition of the low emission mortars tested

Sample	Composition						
	CEM I 42.5R	Fly ash	$CaCO_3$	Slag	Ground components	Water	Quartz sand
	CEM	FA	CC	SL	M		
	(g)	(g)	(g)	(g)	(g)	(mL)	(g)
1	288.0	162.0	–	–	–	225	1350
2	175.5	45.0	–	229.5	–		
3	175.5	–	45.0	229.5	–		
1MAN	288.0	–	–	–	162.0 (FA + AN)		
2MAN	175.5	–	–	229.5	45.0 (FA + AN)		
3MAN	175.5	–	–	229.5	45.0 (CC + AN)		
1MP25	288.0	–	–	–	162.0 (FA + P25)		
2MP25	175.5	–	–	229.5	45.0 (FA + AN)		
3MP25	175.5	–	–	229.5	45.0 (CC + P25)		
REF	450.0	–	–	–	–		

AN – TiO_2 – anatase form; P25 – TiO_2 – Aeroxide® P25

strength was determined by applying a centrally positioned load via a loading roller at a constant rate of 50 ± 10 N/s until failure occurred. Subsequently, the compressive strength of each fractured half was evaluated by applying a load (loading rate: 2.4 ± 0.2 kN/s) to a 40 mm × 40 mm surface area until specimen failure.

2.4.3. Scanning electron microscopy

Microstructural analysis of cement composites was performed with a TESCAN VEGA3 SEM (Brno, Czech Republic) to assess structural homogeneity. Mortar samples, obtained after mechanical strength testing, were manually fractured into ~ 1 cm^2 pieces with flat surfaces, then dried at 105°C for 24 h before imaging.

2.5. Photocatalytic activity

To evaluate the photocatalytic activity of the obtained cementitious composites, specimens with dimensions of 40 mm × 40 mm × 5 mm were immersed in 50 mL of phenol solution (10 mg/L), used as a model organic contaminant. The samples were kept in dark for 24 hours under continuous stirring with a magnetic stirrer to assess the extent of phenol adsorption onto the composite surface. This procedure was repeated until the adsorption equilibrium was reached, defined as a variation in phenol concentration not exceeding 5%. Subsequently, the samples were placed in a fresh phenol solution and exposed to ultraviolet irradiation generated by a 50 W chip-on-board LED lamp emitting at a wavelength of 395 nm (Bridgelux, Fremont, California, USA). To ensure stable thermal conditions and effective heat dissipation during photocatalytic testing, the lamp was equipped with an active cooling system comprising an aluminum heat sink and a fan. The intensity of UV irradiation was maintained at 500 ± 10 mW/cm^2. The experiment was conducted over 24 hours, with 3 mL aliquots collected at 6 and 24 hours. The withdrawn solutions were filtered using syringe filters (Macherey-Nagel, Düren, Germany) to remove suspended solids. Phenol concentration in the collected samples was quantified using a Vanquish high-performance liquid chromatography (HPLC) system (Thermo Fisher Scientific, Waltham, Massachusetts, USA), equipped with a C18 column (Accucore C18; particle size 2.6 μm) and a UV-Vis diode array detector (DAD). Chromatographic analysis was performed at a column temperature of 45°C and a flow rate of 0.3 mL/min, using a methanol-water mixture (1:1 v/v) as the mobile phase.

2.6. Carbon footprint analysis

The carbon footprint analysis of the mortars was assessed by calculating the emissivity of different mixtures, considering only raw materials at the product stage (Module A1, based on EN 15804). Modules A2 (transport) and A3 (manufacturing) were excluded due to their similar values and minor impact on cradle-to-gate global warming potential (GWP). Data were sourced from Environmental Product Declarations (EPDs) and OneClickLCA software (expert license, Poznan University of Technology).

2.7. Statistical analysis

The effects of binder composition factors and the presence and type of TiO_2 on the dependent variables (initial and final setting time, flexural and compressive strength, photocatalytic activity, cumulative heat of hydration, and GWP) were evaluated using multivariate analysis of variance (MANOVA) in Statistica (TIBCO Software Inc., version 14.1.0.4). The significance of the effects was determined at a confidence level of p = 0.05.

3. RESULTS AND DISCUSSION

3.1. Particle size distribution

The particle size distribution results obtained for all powder materials are presented in the form of graphs in Fig. 1. The material with the largest particle sizes is blast-furnace slag (see Fig. 1a), with particles distributed in two distinct ranges: 100–250 nm and 500–3500 nm. The investigated Portland cement sample shows particles in the range of 150–2200 nm, while the TiO_2 oxides are in the range of 100–700 nm for P25 and 150–700 nm for AN (see Fig. 1a). In the case of the calcium carbonate sample analyzed, particles were measured in the range of 300–1100 nm. Upon mechanical combination of CC particles with titanium dioxide, a shift in the particle size range was observed as compared to pure CC, resulting in ranges of 150–700 nm for P25 and 200–800 nm for AN (see Fig. 1b). A similar trend was observed for titanium dioxide ground with fly ash, whose initial particle size distribution ranged from 150–400 nm and 950–2600 nm, respectively. After grinding with P25, the resulting powder exhibited particles in the 100–600 nm and 700–2600 nm ranges, whereas in combination with AN, the particles formed a single size range of 300–1100 nm (see Fig. 1c).

The results obtained are in agreement with those reported in the literature – titanium dioxides, like other powdered materials, tend to aggregate and agglomerate, as confirmed in studies [16, 17], where the determined particle sizes for P25 corresponded to a range of 0.3–150 μm [17]. The measured particle size values for Portland cement fall within the ranges reported by Holzer *et al.* [18] and Ferraris and colleagues [19], which ranges from 0.1 to 100 μm.

3.2. Fourier transform infrared spectroscopy

Figure 2 shows the FTIR spectra of all the powder materials used. The spectrum of Portland cement powder, presented in Fig. 2a, is characterized by bands around 1500–1400 cm^{-1} due to the asymmetric vibrations of carbonate groups, which are associated with the presence of calcite and natural calcium carbonate. A broad band in the range of 1100–900 cm^{-1} corresponds to Si-O stretching vibrations, attributed to calcium silicates primarily present in alite (C_3S, tricalcium silicate) and belite (C_2S, dicalcium silicate). A distinct band observed between 600 and 500 cm^{-1} originates from vibrations of calcium silicates and aluminosilicates (Si-O-Al, Si-O-Si). The weak bands at approximately 3600 cm^{-1} and 1650 cm^{-1} are associated with trace amounts of moisture, as indicated by the recorded stretching and bending vibrations, respectively. The presented spectrum for Portland cement is consistent with those previously reported in the literature [20].

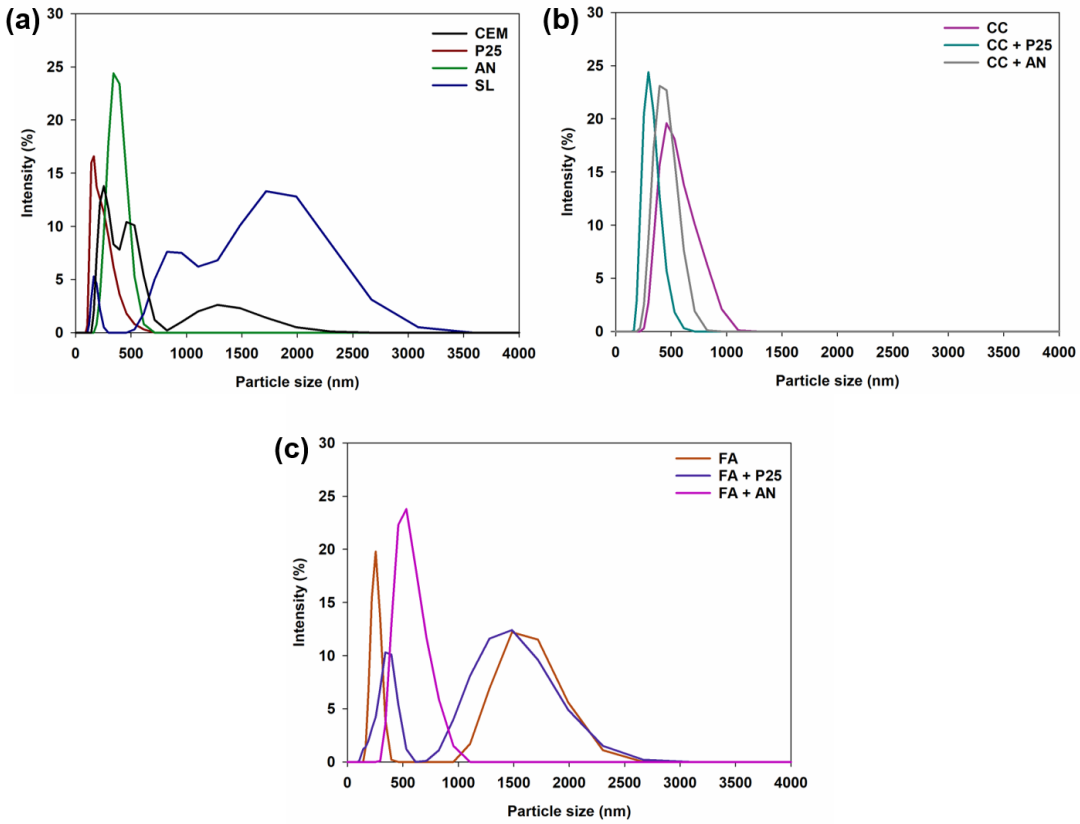

Fig. 1. Particle size distribution of (a) raw components, and raw components ground with TiO_2 based on (b) calcium carbonate and (c) fly ash

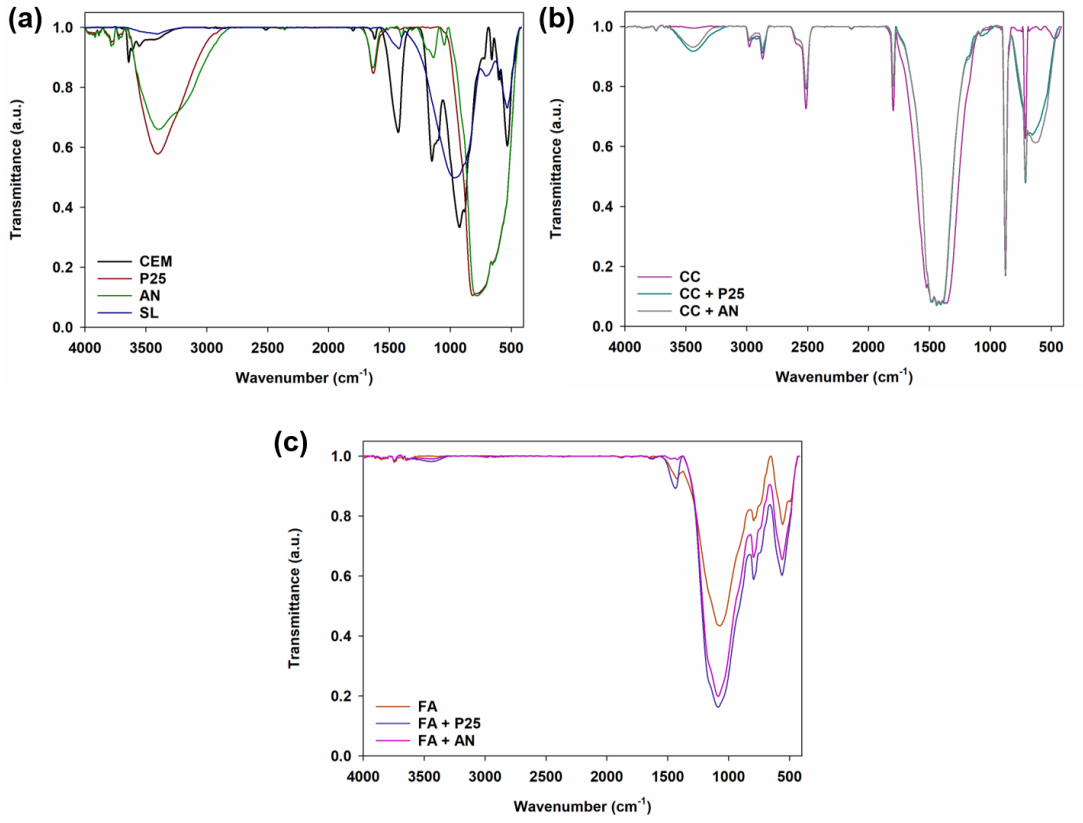

Fig. 2. FTIR spectra of (a) raw components, and raw components ground with TiO_2 based on (b) calcium carbonate and (c) fly ash

The measured FTIR spectra for the titanium dioxides used – both in the P25 and anatase forms – show bands at approximately 3600–3400 cm^{-1}, corresponding to the O-H stretching vibrations of hydroxyl groups, associated with surface-bound or physically adsorbed water. A characteristic broad diffuse band in the range of 700–600 cm^{-1} is attributed to Ti-O and Ti-O-Ti stretching vibrations. The observed peaks in the spectra of titanium dioxides are consistent with those reported in the literature [21]. The spectrum shown in Fig. 2a is complemented by the FTIR spectrum of ground granulated blast furnace slag, in which the most prominent and broad band appears in the range of ~ 1100–800 cm^{-1} and is associated with Si-O and C-O stretching vibrations. Additionally, a band in the ~ 600–500 cm^{-1} region corresponds to framework vibrations of Si-O-Si, Si-O-Al, and Al-O, which are characteristic of aluminosilicates. Similar spectra have also been reported by Metlenkin *et al.* [22] and Deng *et al.* [23], who observed these characteristic bands in the spectra of the slag they investigated. The set of FTIR spectra for calcium carbonate alone and in combination with P25 and AN is presented in Fig. 2b. Analysis of the carbonate bands confirmed that the calcium carbonate used is calcite, as evidenced by the bending bands at approximately 870 cm^{-1} and 700 cm^{-1}, corresponding to out-of-plane and in-plane bending vibrations, respectively. A broad band around 1500 cm^{-1} corresponds to the asymmetric stretching vibrations of the C-O bond, while the band observed at ~ 2500 cm^{-1} is attributed to the vibrations of the carbonate group in calcite. Similar observations have been reported by other researchers in previous studies [24]. The FTIR spectra of carbonates mechanically milled with titanium dioxides confirm the presence of characteristic bands for both calcium carbonate and the corresponding TiO_2. In the set of spectra presented in Fig. 2c, which includes the spectrum of fly ash and the spectra of milled fly ash-TiO_2 systems, three distinct bands characteristic of fly ash can be observed: amorphous aluminosilicates (Si-O-Si and Si-O-Al, ~ 1100–1000 cm^{-1}); crystalline oxide or quartz phases (~ 800 cm^{-1}); and bending vibrations of silicates and aluminosilicates (Si-O-Si, ~ 500 cm^{-1}). These observations are consistent with reports in the literature [25, 26].

3.3. Heat of hydration

Figure 3 presents the hydration heat results of the tested formulations over a 72-hour period as cumulative heat of hydration curves (see Fig. 3a) and heat evolved during the process (see Fig. 3b). The results starting from 1 correspond to samples containing 36% fly ash as clinker replacement, with finely ground TiO_2 in the form of anatase (1MAN) and Aeroxide® P25 (1MP25).

For these systems, a noticeable reduction in hydration heat is observed due to the fine grinding of TiO_2. This grinding process results in a decrease in cumulative hydration heat from nearly 400 J/g to below 300 J/g, as well as a delay in the heat release during the early stages of the setting process. A similar effect was reported by Ślosarczyk *et al.*, who studied AAMs with TiO_2 addition, attributing the reduction in hydration heat to the photocatalytic properties of TiO_2 [27]. Cumulative hydration heat of approximately 300 J/g was also achieved by the sample

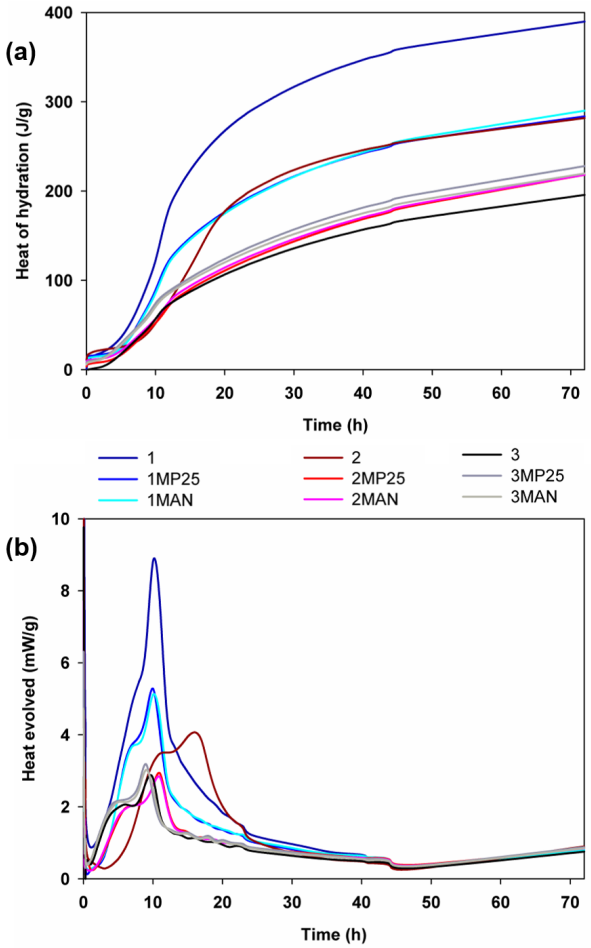

Fig. 3. Heat of hydration results determined by the semi-adiabatic method for all tested composites presented as (a) cumulative heat of hydration curves and (b) heat evolved

in which 51% of the clinker was replaced with slag and 10% with fly ash, labeled as 2. Although this sample exhibited an even greater delay in setting during the early phase – i.e. within the first 10 hours – it also showed an acceleration of hydration within the first hour of testing, similar to the findings in [28]. This early acceleration may contribute to the more stable formation of hydration products such as ettringite. The replacement of pure fly ash with finely ground TiO_2-containing material (samples 2MAN and 2MP25) resulted in a reduction of cumulative hydration heat to approximately 200 J/g, regardless of the TiO_2 form used. In contrast, the use of calcium carbonate with finely ground TiO_2 instead of fly ash (samples 3MAN and 3MP25) led to a slight acceleration in hydration heat release during the first 10 hours and a slightly higher cumulative hydration heat as compared to samples 2MAN and 2MP25, particularly for the P25 form.

Notably, the use of 51% slag combined with 10% calcium carbonate without TiO_2 addition (sample 3) significantly delayed the initial setting and the onset of hydration, extending it beyond 20 hours. This sample also exhibited the lowest cumulative hydration heat measured after 72 hours. Interestingly, studies have shown that adding $CaCO_3$ to Portland cement (without slag)

increases the released hydration heat [12, 29]. The conducted study demonstrates that the applied formulations effectively reduce the hydration heat of the binder without negatively affecting mechanical strength.

Reducing the heat of hydration can improve the durability of cement mortar by promoting a more compact microstructure, which reduces water absorption and limits chloride diffusion [30]. In addition, it protects the mortar from early-age shrinkage and cracking [31].

Additionally, Table 3 presents the initial and final setting times derived from the heat of hydration results. The data show that the incorporation of the ground fly ash-TiO_2 system accelerates both the initial and final setting times, regardless of the type of titanium dioxide used. A reduction in the fly ash content in the composite further shortens the setting period. The addition of slag and calcium carbonate to the system mitigates the setting delay effect even more effectively. These findings are consistent with previous studies in the literature, which have analyzed the influence of calcium carbonate on the hydration behavior of cementitious composites [12, 13].

Table 3
Initial and final setting times of all tested mortars

Sample	Initial setting time [h]	Final setting time [h]
1	6.0	10.0
2	8.4	16.0
3	3.9	10.0
1MAN	5.1	10.0
2MAN	4.2	11.0
3MAN	3.2	9.0
1MP25	5.0	10.0
2MP25	4.8	11.0
3MP25	3.2	9.0

3.4. Physico-mechanical and structural characterization of cement composites

The strength tests were conducted at three different time intervals: early strength at 3 days, standard testing for cement mortars at 28 days, and long-term strength assessment at 150 days.

The results of the flexural strength test are shown in Fig. 4a. For formulation 1, grinding fly ash together with AN and P25 resulted in an increase in flexural strength by approximately 30% at 28 days and 20% at 150 days as compared to samples containing only fly ash. Samples in group 2, which included slag, exhibited comparable flexural strength regardless of whether the fly ash was ground with AN or P25. In this case, the addition of ground fly ash with AN and P25 had no significant influence on flexural strength development. However, it is noteworthy that the 3-day strength of all slag-containing samples was lower than that of samples without slag (1, 1MP25, and 1MAN).

At 28 days, the results for slag-containing samples were higher than those for samples with unmodified fly ash (1, 1MP25, 1MAN) but approximately 12% lower than those for samples with fly ash ground with AN or P25. At 150 days, the flexural strength of the slag-containing samples was comparable to that of samples with unmodified fly ash.

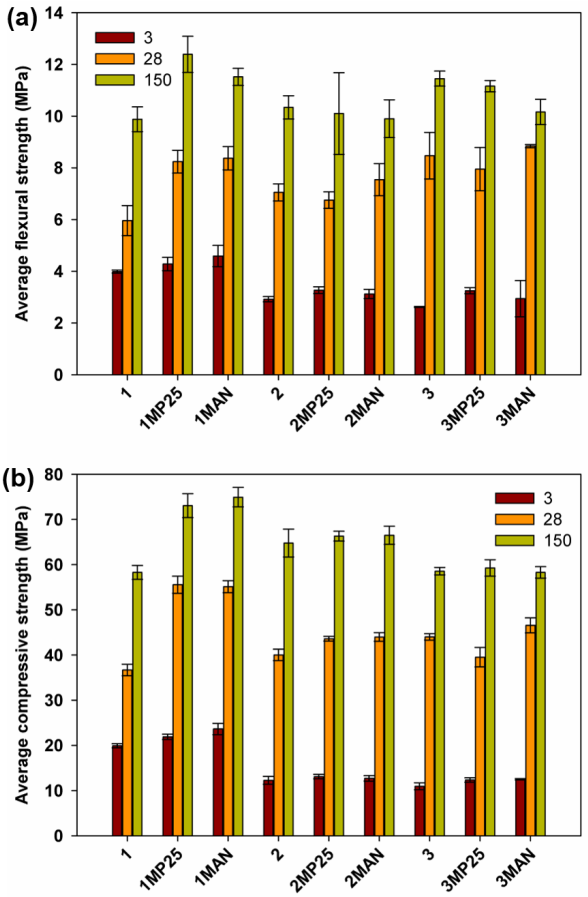

Fig. 4. Mechanical strength results after 3, 28 and 150 days of maturing for all tested composites: (a) average flexural strength and (b) average compressive strength, respectively

Samples in which fly ash was replaced with calcium carbonate (3, 3MP25, 3MAN) exhibited similar flexural strength at 3 days to samples containing fly ash (2, 2MP25, 2MAN). However, after 28 and 150 days, the flexural strength of the calcium carbonate-containing samples was higher than that of the fly ash-based samples, with no significant differences observed between AN- and P25-containing formulations.

With regard to the compressive strength results, which are shown in Fig. 4b, a positive effect of grinding P25 and AN together with fly ash was observed; however, the specific form of TiO_2 did not have a significant impact on the final strength. The compressive strength of samples containing TiO_2 was approximately 45% higher at 28 days and 30% higher at 150 days as compared to the sample without TiO_2.

A similar positive effect of TiO_2 mixed with fly ash on compressive strength was also reported in study [32], which attributed this improvement to enhanced hydration processes and the formation of C-S-H groups with longer chains and a higher Al:Si ratio. Samples containing slag as a clinker replacement (2) exhibited lower early compressive strength; however, their

strength at 28 and 150 days was higher than that of samples with fly ash without TiO_2 (1) but lower than that of samples with finely ground TiO_2 (1MAN, 1MP25).

The negative impact of slag on early compressive strength (at 3 and 7 days) and its positive effect on later strength development (at 56, 84, or 90 days) has been documented in numerous previous studies [33, 34]. It is worth noting that samples containing slag and calcium carbonate (3, 3MAN, 3MP25) achieved compressive strength comparable to those containing slag and fly ash (2, 2MAN, 2MP25) at 28 days. However, after 150 days, their compressive strength was 12% lower.

The positive effect of $CaCO_3$ substitution on the compressive strength of cementitious composites has also been demonstrated in study [35], which investigated the reactivity of calcium carbonate derived from ground oyster shells or limestone filler in combination with GGBS. The studies conducted demonstrated the beneficial effect of grinding fly ash with TiO_2 on the compressive strength of cementitious composites, as well as the positive impact of replacing fly ash with slag combined with either fly ash or calcium carbonate as compared to samples containing only fly ash. However, the most favorable system in terms of compressive strength was the one in which cement was replaced with fly ash ground with TiO_2.

3.5. SEM analysis

Microstructural images of the cement composites examined are presented in Fig. 5. SEM analysis revealed clearly visible unreacted fly ash particles, which can be observed in Fig. 5a–c. In the case of Series 2 composites, in which slag – alongside clinker – acts as the dominant component, slag particles are most prominently visible in Fig. 5d. Upon introducing the ground fly ash-TiO_2 system into the matrix, the composite structure becomes more homogeneous. Figure 5g–i presents the microstructural images of composites containing calcium carbonate.

The visualized structure appears relatively dense and uniform, with no visible air voids. When comparing composites incorporating different forms of titanium dioxide – P25 and AN – it is evident that AN-based systems exhibit a denser and more ho-

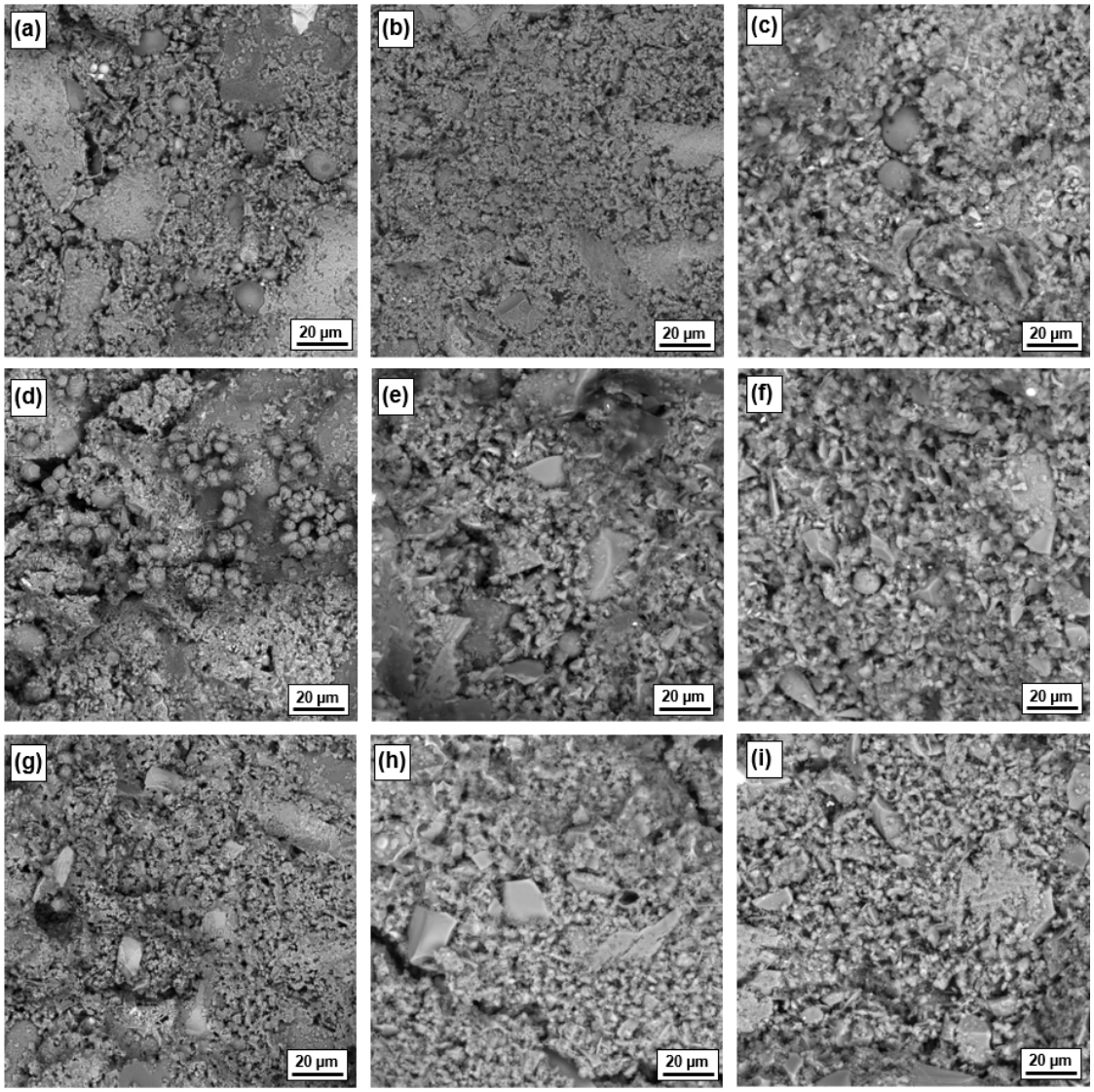

Fig. 5. SEM images of all analyzed cement composites: (a) 1, (b) 1MP25, (c) 1MAN, (d) 2, (e) 2MP25, (f) 2MAN, (g) 3, (h) 3MP25 and (i) 3MAN

mogeneous microstructure. This effect may be attributed to the particle size of this TiO_2 form. As reported in the literature [36], the incorporation of nano-oxides into the cement matrix leads to the formation of active centers that promote the hydration process, thereby contributing to microstructural densification through the formation of hydration products.

3.6. Photocatalytic activity

To evaluate the photocatalytic activity of cementitious composites produced through partial replacement of Portland cement with fly ash, ground granulated blast furnace slag, or calcium carbonate, and incorporating titanium dioxide nanoparticles, a degradation test of a model organic contaminant – phenol – was conducted under UV irradiation at a wavelength of 395 nm. The results are presented in Fig. 6. When analyzing the data obtained from the photocatalytic activity tests, it should be emphasized that the experiments were conducted under specific environmental conditions. Namely, the reaction system contained only a single model contaminant, phenol, and the tests were performed exclusively under ultraviolet irradiation. Phenol was selected as the model organic pollutant because phenol and its derivatives are widespread environmental contaminants, and the mechanism of their photocatalytic degradation in the presence of TiO_2 powder under UV light has been well documented in the literature [37].

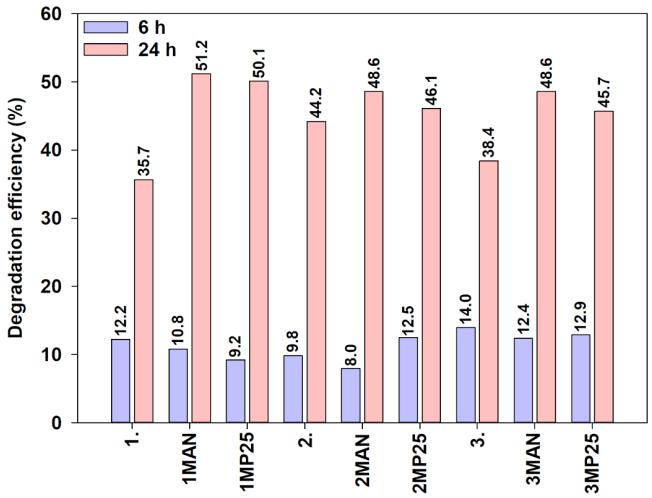

Fig. 6. Results of the effectiveness of model tests on the degradation of organic pollutants under the influence of UV radiation for the cement composites tested

The primary objective of the photocatalytic activity tests was to evaluate how variations in composite composition influenced photocatalytic performance; therefore, a pure phenol solution was employed. These conditions do not reflect real environmental systems, where phenol typically coexists with other organic and inorganic pollutants that may interfere with the photocatalytic process and contribute to water-phase turbidity, thereby reducing the amount of radiation reaching the composite surface. Nevertheless, using a pure phenol solution allowed the experiments to be conducted under uniform conditions, enabling reliable comparisons between individual composites. Visible-light irradiation was deliberately excluded, as one of the photocatalysts used was pure anatase, which in its pristine form exhibits limited activity under visible light due to its band gap of 3.2 eV [38].

As the data indicate, all tested samples exhibited a significant increase in phenol degradation efficiency with prolonged UV exposure, from 6 to 24 hours. Moreover, the incorporation of TiO_2 into the cement matrix enhanced photocatalytic activity, both in the form of pristine anatase (AN) and the commercial anatase-rutile mixture (P25). However, higher degradation efficiencies were observed in samples containing only anatase. The degradation efficiencies for samples 1MAN, 2MAN, and 3MAN were 51.2%, 48.6%, and 48.6%, respectively. For the P25-based samples – 1MP25, 2MP25, and 3MP25 – the values were 50.1%, 46.1% and 45.7%, respectively. Similar trends were observed in our previous studies [39]. The observed reduction in phenol concentration is attributed to the photocatalytic mechanism, which relies on the simultaneous presence of TiO_2 nanoparticles and their exposure to UV light of the appropriate wavelength [39]. The effectiveness of TiO_2-modified photocatalytic cement composites has also been confirmed in other studies [40]. It is noteworthy that in photocatalytic tests conducted on the powders alone – prior to their incorporation into the cement matrix – the P25 variant typically demonstrates superior activity [15, 39]. In the case of composites without the intentional addition of TiO_2 nanoparticles, the observed photocatalytic behavior may be due to the inherent TiO_2 content in the supplementary materials used, namely fly ash and slag. X-ray fluorescence analysis revealed TiO_2 contents of 1.51% and 0.72%, respectively. Xu *et al.* [39] demonstrated that the fly ash content influences the microstructure of TiO_2-modified composites, particularly by increasing the cumulative pore volume. This enhanced porosity improves the exposure of TiO_2 nanoparticles to UV light and facilitates greater interaction with water molecules, resulting in elevated formation of hydroxyl radicals. These radicals play a key role in the degradation of both aqueous and airborne organic pollutants.

3.7. Carbon footprint analysis

GWP (Global Warming Potential) was calculated for all formulations and the results of the analysis are shown in Fig. 7. To show the pro-environmental impact of the modifications made to the mortar compositions, the results are compared with GWP of a standard mortar based on 100% Portland cement /REF/.

From the analysis, it was noted that for group 1, replacing the Portland cement with 36% FA results in a 35% decrease in GWP, and using TiO_2 in addition increases GWP by 8%, but it is still 30% lower than the reference sample. In contrast, the use of 51% slag instead of Portland cement and 10% FA or $CaCO_3$ (samples 2 and 3), results in a GWP reduction of 30% relative to sample 1, and a reduction of as much as 55% relative to the reference sample with Portland cement. Also in the case of slag-containing samples, the use of FA or $CaCO_3$ doped with TiO_2 (samples 2MAN, 2MP25, 3MAN, 3MP25) results in an increase in GWP, but this is an increase of only 12% relative to samples without TiO_2, and when compared to the reference

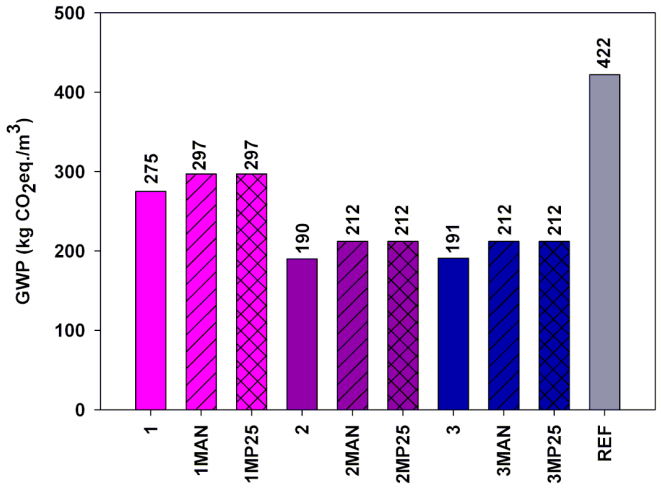

Fig. 7. Calculated Global Warming Potential values for all systems analyzed

sample, GWP is still 50% lower and 29% lower than the samples without slag (1MAN, 1MP25). Other researchers point out that the use of waste materials such as fly ash or GGBS as substitutes for clinker, in addition to lowering the emissivity of the mortar, also solves the problem of waste disposal, the high cost of clinker production and its environmental impact [41]. Still other researchers have shown that replacing Portland cement (OPC) with 50% to 70% GGBS or FA can result in a reduction in total environmental impacts by 44% to 61% [42]. In contrast, further researchers have shown that using 65% GGBS and 50% FA can reduce GWP by 61% and 54% as compared to using OPC [43].

4. DISCUSSION

A multivariate analysis of variance (MANOVA) was performed on the obtained results using the Statistica software to determine the influence of individual factors (binder composition, and the presence and form of TiO_2) on the variables measured. The results of this analysis are presented in Table 4.

The analysis showed that the presence and type of TiO_2 accounted for 52% of the variation at the start and end of the setting time. In contrast, the binder composition had a 94% influence on the compressive strength after 3 days. Interestingly, the standard compressive strength measured after 28 days was most affected by the interaction between binder composition and the type of TiO_2 used, accounting for 44% of the observed variation. For compressive strength measured after 150 days, binder composition again exerted the greatest influence, although to a lesser extent than at 3 days, contributing 45% of the variation.

The photocatalytic properties after 6 hours were influenced in 48% by binder composition, in 13% by TiO_2, and in 39% by the interaction between binder composition and the presence and type of TiO_2. After 24 hours, photocatalytic activity was 76% dependent on TiO_2 and 21% on the interaction between factors.

Regarding the heat of hydration, the presence and type of TiO_2 accounted for 72% of the variation, while the interaction between binder composition and TiO_2 contributed 25%. For GWP, binder composition had the predominant effect, accounting for 94% of the variation.

Table 4
Percentage contribution of each input variable to variance, as determined by ANOVA

Variable	Binder composition [%]	Presence and form of TiO_2 [%]	Interaction [%]
Initial setting time	31	52	17
Final setting time	22	52	26
Flexural strength at 3 days	83	8	5
Compressive strength at 3 days	94	3	1
Flexural strength at 28 days	28	20	29
Compressive strength at 28 days	21	31	44
Flexural strength at 150 days	23	10	36
Compressive strength at 150 days	45	19	28
Photocatalytic activity at 6 h	48	13	38
Photocatalytic activity at 24 h	3	76	21
Cumulative heat of hydration	3	72	25
GWP	94	6	0

Looking ahead, the authors highlight the potential of machine learning (ML) to reduce the amount of laboratory testing required. ML techniques are increasingly applied in the testing and evaluation of cement composites, offering significant advantages in predicting various properties and behaviors of these materials with high accuracy and efficiency. Machine learning has been successfully used to predict compressive strength, pull-off adhesion, and the effects of additives such as eggshell powder and recycled glass powder on cement composites [44–46]. In particular, artificial neural network (ANN) models have demonstrated exceptional accuracy in predicting the mechanical properties of mortars, with the error between predicted and experimental values as low as 1.32% [46].

5. CONCLUSIONS

This study presents an original approach to the development of low-emission cement composites with photocatalytic properties, utilizing materials such as ground granulated blast furnace slag, calcium carbonate and fly ash. The proposed method, which involves co-grinding fly ash and/or calcium carbonate with TiO_2, effectively prevents potential aggregation and agglomeration of TiO_2 particles. The materials produced through this method exhibit weak interactions between fly ash-TiO_2 and calcium carbonate-TiO_2 systems, as confirmed by FTIR analysis. The incorporation of these systems into low-emission cement composites mitigated the setting delay effect, accelerating both the initial and final setting times when compared to reference systems. Furthermore, the proposed composite formulations re-

sulted in a reduction of cumulative hydration heat by up to 50%. Mechanical property testing demonstrated the beneficial effect of the introduced additives, yielding average flexural and compressive strengths that were comparable to or significantly higher than those of the reference composites. The proposed cement composites exhibit a reduced environmental impact, effectively contributing to CO_2 emission reduction. Additionally, all TiO_2-containing configurations demonstrated photocatalytic activity under UV light, with the most favorable results observed for materials incorporating TiO_2 in the anatase form.

Considering the photocatalytic properties of the mortars, they could be applied as surface materials, such as external plasters or cladding boards. Therefore, characteristics such as reduced heat of hydration are desirable, as they limit the formation of early-age cracks and consequently improve both the durability and aesthetic quality of the material. In addition, when the material is used as plaster, the delayed setting time extends the pot life of the fresh mortar, facilitating easier application.

For further research, it would be beneficial to examine the size and volume of air pores in the composites produced, to assess their durability, and to manufacture finished building elements, such as paving slabs or façade panels.

DECLARATION OF COMPETING INTEREST

The authors declare that they have no known competing financial interests or personal relationships that could have appeared to influence the work reported in this paper.

ACKNOWLEDGEMENTS

This work was supported by the subsidy from the Polish Minister of Science and Higher Education under Research Project No. 0412/SIGR/6579 and 0412/SBAD/0091.

DATA AVAILABILITY

Data will be made available on request.

REFERENCES

[1] G.F. Huseien *et al.*, "Evaluation of high-volume fly-ash cementitious binders incorporating nanosilica as eco-friendly sustainable repair materials," *Constr. Build. Mater.*, vol. 447, p. 138022, 2024, doi: 10.1016/j.conbuildmat.2024.138022.

[2] H. Zhang, X. Wang, and P. Hao, "Effects of fly ash content on the strength property of cement concrete pavement," *Appl. Mech. Mater.*, vol. 174–177, pp. 403–408, 2012, doi: 10.4028/www.scientific.net/AMM.174-177.403.

[3] P.Z. Razi and H.A. Razak, "Environmental sustainability and engineering performance of self-compacting mortar incorporating fly ashes," *Appl. Mech. Mater.*, vol. 253–255, pp. 559–563, 2013, doi: 10.4028/www.scientific.net/AMM.253-255.559.

[4] Z.H. Naji, H.M. Mubarak and A.M. Ibrahim, "The effect of height replacement fly ash on properties of mortar," *Ann. Chim. – Sci. Mat.*, vol. 49, pp. 43–48, 2025, doi: 10.18280/acsm.490106.

[5] Y. Han and R.-S. Lin, "Compressive strength estimation and CO_2 reduction design of fly ash composite concrete," *Buildings*, vol. 12, p. 139, 2022, doi: 10.3390/buildings12020139.

[6] S. Aydin, C. Karatay, and B. Baradan, "The effect of grinding process on mechanical properties and alkali-silica reaction resistance of fly ash incorporated cement mortars," *Powder Technol.*, vol. 197, pp. 68–72, 2010, doi: 10.1016/j.powtec.2009.08.020.

[7] L. Coppola, D. Coffetti, and E. Crotti, "Rheological and physical performances of mortars manufactured with plain and ultrafine fly ashes," *ACI Special Publication*, vol. 2018, p. 142064, 2018, doi: 10.14359/51711014.

[8] A.I. Ruiz, M.A. de la Rubia, J. Massana, F. Alonso Peralta, A. Moragues and E. Reyes, "Sustainable low-cement blends featuring blast-furnace slag, metakaolin and nanosilica show remarkable long-term durability against chlorides for one day curing age," *Case Stud. Constr. Mater.*, vol. 22, p. e04511, 2025, doi: 10.1016/j.cscm.2025.e04511.

[9] X. Luo, J. Kim, and Y. Hama, "Microstructural changes in blast-furnace cements with different replacement ratios under repeated drying and wetting cycles," *J. Build. Eng.*, vol. 100, p. 111763, 2025, doi: 10.1016/j.jobe.2024.111763.

[10] A. Król and Z. Giergiczny, "Properties of concrete made with low-emission cements CEM II/C-M and CEM VI," *Materials*, vol. 13, p. 2257, 2020, doi: 10.3390/ma13102257.

[11] F.U.A. Shaikh and S.W.M. Supi, "Compressive strength and durability of high-volume fly ash concrete reinforced with calcium carbonate nanoparticles," in *Fillers and Reinforcements for Advanced Nanocomposites*, Y. Dong, R. Umer, A. Kin-Tak Lau (eds), Woodhead Publishing.

[12] M. Aqel and D.K. Panesar, "Hydration kinetics and compressive strength of steam-cured cement pastes and mortars containing limestone," *Constr. Build. Mater.*, vol. 113, pp. 359–368, 2016, doi: 10.1016/j.conbuildmat.2016.03.031.

[13] L. Coppola, D. Coffetti, E. Crotti, R. Dell'Aversano, G. Gazzaniga, and T. Pastore, "Influence of lithium carbonate and sodium carbonate on physical and elastic properties and on carbonation resistance of calcium sulphoaluminate-based mortars," *Appl. Sci.*, vol. 10, p. 176, 2020, doi: 10.3390/app10010176.

[14] D. Chen *et al.*, "Photocatalytic degradation of organic pollutants using TiO_2-based photocatalysts: A review," *J. Clean. Prod.*, vol. 268, p. 121725, 2020, doi: 10.1016/j.jclepro.2020.121725.

[15] P. Jędrzejczak *et al.*, "Carbon-modified TiO_2 as a promising and efficient admixture for cementitious composites: A comprehensive study of photocatalytic, mechanical and structural properties," *J. Build. Eng.*, vol. 78, 107747, 2023, doi: 10.1016/j.jobe.2023.107747.

[16] A. Brunelli, G. Pojana, S. Callegaro, and A. Marcomini, "Agglomeration and sedimentation of titanium dioxide nanoparticles (n-TiO_2) in synthetic and real waters," *J. Nanoparticle Res.*, vol. 15, p. 1684, 2013, doi: 10.1007/s11051-013-1684-4.

[17] M. Rajca, R.T. Bray, and A. Sokołowska, "Granulometric analysis of TiO_2 particles in the aspect of membrane filtration," *Desal. Water Treat.*, vol. 316, pp. 583–588, 2023, doi: 10.5004/dwt.2023.30175.

[18] L. Holzer, R.J. Flatt, S.T. Erdogan, J.W. Bullard, and E.J. Garboczi, "Shape comparison between 0.4-2.0 and 20-60 µm cement particles," *J. Am. Cer. Soc.*, vol. 93, pp. 1626–1633, 2010, doi: 10.1111/j.1551-2916.2010.03654.x.

[19] C.F. Ferraris, V.A. Hackley, and A.I. Aviles, "Measurement of particle size distribution in Portland cement powder: Analysis of ASTM round robin studies," *Cem. Concr. Aggr.*, vol. 26, pp. 71–81, 2004, doi: 10.1520/cca11920.

[20] H.K. Choudhary *et al.*, "Observation of phase transformations in cement during hydration," *Constr. Build. Mater.*, vol. 101, pp. 122–129, 2015, doi: 10.1016/j.conbuildmat.2015.10.027.

[21] S. Saravanan and R.S. Dubey, "Optical and morphological studies of TiO_2 nanoparticles prepared by sol-gel method," *Mater. Today Proc.*, vol. 47, pp. 1811–1814, 2021, doi: 10.1016/j.matpr.2021.03.207.

[22] D.A. Metlenkin *et al.*, "Identification of the elemental composition of granulated blast furnace slag by FTIR-Spectroscopy and chemometrics," *Processes*, vol. 10, p. 2166, 2022, doi: 10.3390/pr10112166.

[23] J. Deng, G. Wu, Y. Xia, and L. Liu, "Preparation and hydration properties of sodium silicate-activated municipal solid waste incineration bottom ash composite ground-granulated blast furnace slag cementitious materials," *Materials*, vol. 17, p. 2406, 2024, doi: 10.3390/ma17102406.

[24] N. Nurhayati, E.H. Sujiono, V. Zharvan, M. Saleh, A.T. Awiseng, and M.F. Nursetya, "Synthesis of precipitated calcium carbonate (PCC) as a raw paramagnetic material based on ferrite-calcite (Fe-$CaCO_3$) and its potential application," *J. Phys. Conf. Ser.*, vol. 1899, p. 012122, 2021, doi: 10.1088/1742-6596/1899/1/012122.

[25] J. Yang, H. Sun, T. Peng, L. Zeng, and L. Chao, "Study on the overall reaction pathways and structural transformations during decomposition of coal fly ash in the process of alkali-calcination," *Materials*, vol. 14, p. 1163, 2021, doi: 10.3390/ma14051163.

[26] S. Kumar, G. Mucsi, F. Kristály, and P. Pekker, "Mechanical activation of fly ash and its influence on micro and nano-structural behavior of resulting geopolymers," *Adv. Powder Technol.*, vol. 28, pp. 805–813, 2017, doi: 10.1016/j.apt.2016.11.027.

[27] A. Ślosarczyk, I. Klapiszewska, P. Jędrzejczak, W. Jędrzejczak, and Ł. Klapiszewski, "Synthesis and characterization of eco-efficient alkali-activated composites with self-cleaning properties for sustainable construction," *Molecules*, vol. 28, p. 6066, 2023,doi: 10.3390/molecules28166066.

[28] C. Wang, C. Yang, J. Qian, M. Zhong, and S. Zhao, "Behavior and mechanism of pozzolanic reaction heat of fly ash and ground granulated blast furnace slag at early age," *Kuei Suan Jen Hsueh Pao J. Chin. Ceram. Soc.*, vol. 40, pp. 1050–1058, 2012.

[29] S.H. Liu and L. Wang, "Influence of limestone powder on hydration properties of complex binders," *Mater. Res. Innov.*, vol. 18, pp. 2186–2190, 2014, doi: 10.1179/1432891714Z.000000000624.

[30] S. Nie, W. Zhang, S. Hu, Z. Liu, and F. Wang, "Improving the fluid transport properties of heat-cured concrete by internal curing," *Constr. Build. Mater.*, vol. 168, pp. 522–531, 2018, doi: 10.1016/j.conbuildmat.2018.02.068.

[31] D.P. Bentz and M.A. Peltz, "Reducing thermal and autogenous shrinkage contributions to early-age cracking," *ACI Mater. J.*, vol. 105, pp. 414–420, 2008.

[32] B. Ma, H. Li, X. Li, J. Mei, and Y. Lv, "Influence of nano-TiO_2 on physical and hydration characteristics of fly ash–cement systems," *Constr. Build. Mater.*, vol. 122, pp. 242–253, 2016, doi: 10.1016/j.conbuildmat.2016.02.087.

[33] C.M. Yun, M.R. Rahman, C.Y.W. Phing, A.W.M. Chie, and M.K.B. Bakri, "The curing times effect on the strength of ground granulated blast furnace slag (GGBFS) mortar," *Constr. Build. Mater.*, vol. 260, p. 120622, 2020, doi: 10.1016/j.conbuildmat.2020.120622.

[34] N. Zhang, Q. Fu, J. Wang, L. Lu, Q. Luo, and F. Xing, "Compressive strength and chloride permeability of cement-based materials with high-volume compound mineral admixtures," *Adv. Cem. Res.*, vol. 36, pp. 531–539, 2024, doi: 10.1680/jadcr.23.00185.

[35] W. Deboucha *et al.*, "Reactivity effect of calcium carbonate on the formation of carboaluminate phases in ground granulated blast furnace slag blended cements," *Sustainability*, vol. 13, p. 6504, 2021, doi: 10.3390/su13116504.

[36] K.M. Arsalan, I.M. Khalid, K. Irshad, H.M. Ali, M.A. Hasan, and S. Islam, "Comparative overview of the performance of cementitious and non-cementitious nanomaterials in mortar at normal and elevated temperatures," *Nanomaterials*, vol. 11, p. 911, 2021, doi: 10.3390/nano11040911.

[37] S. Ahmed, M.G. Rasul, W.N. Martens, R. Brown, and M.A. Hashib, "Heterogeneous photocatalytic degradation of phenols in wastewater: A review on current status and developments," *Desalination*, vol. 261, pp. 3–18, 2010, doi: 10.1016/j.desal.2010.04.062.

[38] T.J. Pawar, D.C. López, J.L.O. Romero, and J. Vallejo, "Surface modification of titanium dioxide," *J. Mater. Sci.*, vol 58, pp. 6887–6930, 2023, doi: 10.1007/s10853-023-08439-x.

[39] M. Xu *et al.*, "Effect of TiO_2 and fly ash on photocatalytic NO_x abatement of engineered cementitious composites," *Constr. Build. Mater.*, vol. 236, p. 117559, 2020, doi: 10.1016/j.conbuildmat.2019.117559.

[40] P. Jędrzejczak *et al.*, "The influence of various forms of titanium dioxide on the performance of resultant cement composites with photocatalytic and antibacterial functions," *Mater. Res. Bull.*, vol. 160, p. 112139, 2023, doi: 10.1016/j.materresbull.2022.112139.

[41] S.A. Mahevi, A.K. Kaliluthin, D. Husain, Y. Ansari, and I. Ahmad, "Ecological footprint and economic assessment of ready-mix concrete production," in *Environmental Footprints and Eco-design of Products and Processes*, S.S. Muthu (ed.), Springer Cham, 2024, doi: 10.1007/978-3-031-69047-1_4.

[42] M.K.H. Radwan, C.C. Onn, K.H. Mo, S.P. Yap, R.J. Chin, and S.H. Lai, "Sustainable ternary cement blends with high-volume ground granulated blast furnace slag–fly ash," *Environ. Dev. Sustain.*, vol. 24, pp. 4751–4785, 2022, doi: 10.1007/s10668-021-01633-4.

[43] C. Orozco, S. Babel, S. Tangtermsirikul, and T. Sugiyama, "Comparison of environmental impacts of fly ash and slag as cement replacement materials for mass concrete and the impact of transportation," *Sustain. Mater. Technol.*, vol. 39, p. e00796, 2024, doi: 10.1016/j.susmat.2023.e00796.

[44] S. Czarnecki, Ł. Sadowski, and J. Hoła, "Evaluation of interlayer bonding in layered composites based on non-destructive measurements and machine learning: Comparative analysis of selected learning algorithms," *Autom. Constr.*, vol. 132, p. 103977, 2021, doi: 10.1016/j.autcon.2021.103977.

[45] G. Nakkeeran, L. Krishnaraj, A. Bahrami, H. Almujibah, H. Panchal, and M.M.A. Zahra, "Machine learning application to predict the mechanical properties of glass fiber mortar," *Adv. Eng. Softw.*, vol. 180, p. 103454, 2023, doi: 10.1016/j.advengsoft.2023.103454.

[46] F. Zhu, X. Wu, Y. Lu and J. Huang, "Strength reduction due to acid attack in cement mortar containing waste eggshell and glass: A machine learning-based modeling study," *Buildings*, vol. 14, p. 225, 2024, doi: 10.3390/buildings14010225.